

# Observing $H \rightarrow W^{(*)}W^{(*)} \rightarrow e^{\pm}\mu^{\mp}\cancel{p}_T$ in weak boson fusion with dual forward jet tagging at the CERN LHC

D. Rainwater and D. Zeppenfeld

*Department of Physics, University of Wisconsin, Madison, WI 53706*

Weak boson fusion promises to be a copious source of intermediate mass Standard Model Higgs bosons at the LHC. The additional very energetic forward jets in these events provide for powerful background suppression tools. We analyze the  $H \rightarrow W^{(*)}W^{(*)} \rightarrow e^{\pm}\mu^{\mp}\cancel{p}_T$  decay mode for a Higgs boson mass in the 130-200 GeV range. A parton level analysis of the dominant backgrounds (production of  $W$  pairs,  $t\bar{t}$  and  $Z \rightarrow \tau\tau$  in association with jets) demonstrates that this channel allows the observation of  $H \rightarrow W^{(*)}W^{(*)}$  in a virtually background-free environment, yielding a significant Higgs boson signal with an integrated luminosity of  $5 \text{ fb}^{-1}$  or less. Weak boson fusion achieves a much better signal to background ratio than inclusive  $H \rightarrow e^{\pm}\mu^{\mp}\cancel{p}_T$  and is therefore the most promising search channel in the 130-200 GeV mass range.

## I. INTRODUCTION

The search for the Higgs boson and, hence, for the origin of electroweak symmetry breaking and fermion mass generation, remains one of the premier tasks of present and future high energy physics experiments. Fits to precision electroweak (EW) data have for some time suggested a relatively small Higgs boson mass, of order 100 GeV [1]. This is one of the reasons why the search for an intermediate mass Higgs boson is particularly important [2].

For the intermediate mass range, most of the literature has focussed on Higgs boson production via gluon fusion [2] and  $t\bar{t}H$  [3] or  $WH(ZH)$  [4] associated production. Cross sections for Standard Model (SM) Higgs boson production at the LHC are well-known [2], and while production via gluon fusion has the largest cross section by almost one order of magnitude, there are substantial QCD backgrounds. A search for the very clean four-lepton signature from  $H \rightarrow ZZ$  decay can find a Higgs boson in the mass region  $m_H \gtrsim 130 \text{ GeV}$ , but due to the small branching fraction of this mode very large integrated luminosities, up to  $100 \text{ fb}^{-1}$  or more, are required. One can search for  $gg \rightarrow H$  via  $H \rightarrow W^{(*)}W^{(*)} \rightarrow e^{\pm}\mu^{\mp}\cancel{p}_T$  decays with much lower luminosity [5–7], but with lower signal-to-background ratios.

The second largest production cross section is predicted for weak-boson fusion (WBF),  $qq \rightarrow qqVV \rightarrow qqH$ . These events contain additional information in their observable quark jets. Techniques like forward jet tagging [8–10] can then be exploited to significantly reduce the backgrounds. WBF and gluon fusion nicely complement each other: together they allow for a measurement of the  $t\bar{t}H/WWH$  coupling ratio.

Another feature of the WBF signal is the lack of color exchange between the initial-state quarks. Color coherence between initial- and final-state gluon bremsstrahlung leads to suppressed hadron production in the central region, between the two tagging-jet candidates of the signal [11]. This is in contrast to most background processes, which typically involve color exchange in the  $t$ -channel and thus lead to enhanced hadronic activity between the tagging jets. We exploit these features, via a veto of soft jet activity in the central region [7].

While some attention has been given to intermediate-mass  $H \rightarrow W^{(*)}W^{(*)}$  searches at the LHC in the framework of gluon fusion [5,6], production via weak boson fusion for the same decay mode has not yet been discussed in the literature. Thus, we provide a first analysis of intermediate-mass  $VV \rightarrow H \rightarrow W^{(*)}W^{(*)}$  at the LHC (and of the main physics and reducible backgrounds) which demonstrates the feasibility of Higgs boson detection in this channel, with very low luminosity.  $H \rightarrow W^{(*)}W^{(*)}$  event characteristics are analyzed for dual leptonic decays to  $e^{\pm}\mu^{\mp}$  only, to avoid backgrounds from  $Z, \gamma \rightarrow e^+e^-, \mu^+\mu^-$ .

Our analysis is a parton-level Monte Carlo study, using full tree-level matrix elements for the WBF Higgs signal and the various backgrounds. In Section II we describe our calculational tools, the methods employed in the simulation of the various processes, and important parameters. Extra minijet activity is simulated by adding the emission of one extra parton to the basic signal and background processes. Generically we call the basic signal process (with its two forward tagging jets) and the corresponding background calculations “2-jet” processes, and refer to the simulations with one extra parton as “3-jet” processes. In Section III, using the 2-jet programs for the backgrounds, we demonstrate forward jet tagging, a  $b$  veto and other important cuts which combine to yield

an  $\approx 2/1$  to  $1/2$  signal-to-background (S/B) ratio, depending on the Higgs mass.

In Section IV we analyze the different minijet patterns in signal and background, using both the truncated shower approximation (TSA) [12] to regulate the cross sections, and the gluon exponentiation model to estimate the minijet multiplicity [13]. By exploiting the two most important characteristics of the extra radiation, its angular distribution and its hardness, the QCD backgrounds can be suppressed substantially by a veto on extra central jet emission. Within the TSA and exponentiation models, probabilities are estimated for vetoing signal and background events, and are combined with the production cross sections of the previous section to predict signal and background rates in Table II. These rates demonstrate the feasibility of extracting a very low background  $H \rightarrow W^{(*)}W^{(*)}$  signal at the LHC.

Our signal selection is not necessarily optimized yet. The variables we identify for cuts are the most distinctive, but deserve a multivariate analysis with detector simulation. We do construct an additional variable in Section V which is not used for cuts, but rather can be used to extract the Higgs boson mass from the final event sample.

## II. CALCULATIONAL TOOLS

We simulate  $pp$  collisions at the CERN LHC,  $\sqrt{s} = 14$  TeV. All signal and background cross sections are determined in terms of full tree level matrix elements for the contributing subprocesses and are discussed in more detail below.

For all our numerical results we have chosen  $\sin^2\theta_W = 0.2315$ ,  $M_Z = 91.19$  GeV, and  $G_F = 1.16639 \cdot 10^{-5}$  GeV $^{-2}$ , which translates into  $M_W = 79.94$  GeV and  $\alpha(M_Z) = 128.74$  when using the tree-level relations between these input parameters. This value of  $M_W$  is somewhat lower than the current world average of  $\approx 80.35$  GeV. However, this difference has negligible effects on all cross sections, e.g. the  $qq \rightarrow qqH$  signal cross section varies by about 0.5% between these two  $W$  mass values. The tree level relations between the input parameters are kept in order to guarantee electroweak gauge invariance of all amplitudes. For all QCD effects, the running of the strong coupling constant is evaluated at one-loop order, with  $\alpha_s(M_Z) = 0.118$ . We employ CTEQ4L parton distribution functions [14] throughout. Unless otherwise noted the factorization scale is chosen as  $\mu_f = \min(p_T)$  of the defined jets.

### A. The $qq \rightarrow qqH(g)$ signal process

The signal can be described, at lowest order, by two single-Feynman-diagram processes,  $qq \rightarrow qq(WW, ZZ) \rightarrow qqH$ , *i.e.*  $WW$  and  $ZZ$  fusion where the weak bosons are emitted from the incoming quarks [15]. Because of the small Higgs boson width in the mass range of interest, these events can reliably be simulated in the narrow width approximation. From previous studies of  $H \rightarrow \gamma\gamma$  [16] and  $H \rightarrow \tau\tau$  [17] decays in weak boson fusion we know several features of the signal, which can be exploited here also: the centrally produced Higgs boson tends to yield central decay products (in this case  $W^+W^-$ ), and the two quarks enter the detector at large rapidity compared to the  $W$ 's and with transverse momenta in the 20 to 100 GeV range, thus leading to two observable forward tagging jets.

For the study of a central jet veto, we utilize the results of previous studies where we simulated the emission of at least one extra parton [17,18]. This was achieved by calculating the cross sections for the process  $qq \rightarrow qqHg$ , *i.e.* weak boson fusion with radiation of an additional gluon, and all crossing related processes.

An important additional tool for distinguishing the  $H \rightarrow e^\pm\mu^\mp\not{p}_T$  signal from various backgrounds is the anti-correlation of the  $W$  spins, as pointed out in Ref. [6]. This is due to the preservation of angular momentum in the decay of the spin-0 Higgs boson. Of course, we can observe only the angular distributions of the charged decay leptons, but this is sufficient. The decay rate is proportional to  $(p_{\ell^-} \cdot p_\nu)(p_{\ell^+} \cdot p_{\bar{\nu}})$ . In the rest frame of the Higgs boson, in which the  $e^-\bar{\nu}$  or  $e^+\nu$  pairs are emitted back-to-back for  $W^+W^-$  production at threshold, this product is a maximum for the charged leptons being emitted parallel. This characteristic is preserved and even enhanced when boosted to the lab frame, as the Higgs boson in weak boson fusion is typically emitted with  $p_T \approx 60 - 120$  GeV.

### B. The QCD $t\bar{t} + jets$ backgrounds

Given the H decay signature, the main physics background to our  $e^\pm\mu^\mp\not{p}_T$  signal arises from  $t\bar{t} + jets$  production, due to the large top production cross section at the LHC and because the branching ratio  $B(t \rightarrow Wb)$  is essentially

100%.

The basic process we consider is  $pp \rightarrow t\bar{t}$ , which can be either  $gg$ - or  $q\bar{q}$ -initiated, with the former strongly dominating at the LHC. QCD corrections to this lead to additional real parton emission, *i.e.* to  $t\bar{t} + j$  events. Relevant subprocesses are

$$gg \rightarrow t\bar{t}q, \quad g\bar{q} \rightarrow t\bar{t}\bar{q}, \quad q\bar{q} \rightarrow t\bar{t}g, \quad gg \rightarrow t\bar{t}g, \quad (1)$$

and the subprocesses for  $t\bar{t} + jj$  events can be obtained similarly. For the case of no additional partons, the  $b$ 's from the decaying top quarks may be identified as the tagging jets. In this case, calculating the cross section for  $t\bar{t} + j$  where the  $b$ 's are explicitly identified as the tagging jets serves to estimate the effect of additional soft parton emission, *i.e.* minijet activity in the central detector; this is described in detail in Sec. IV. At the same time, we can identify a distinctly different, perturbative region of phase space, where the final-state light quark or gluon gives rise to one tagging jet, and one of the two decay  $b$ 's is identified as the other tagging jet. In this case,  $t\bar{t} + jj$  may be used to estimate minijet activity for the hard process  $pp \rightarrow t\bar{t} + j$ . Finally, there is a third distinct region of phase space, for the perturbative hard process  $pp \rightarrow t\bar{t} + jj$ , where the final state light quarks or gluons are the two tagging jets.

Thus, the “ $t\bar{t}j$ ” and “ $t\bar{t}jj$ ” calculations serve a dual purpose: to obtain the cross sections for the contribution of the perturbative processes where light quark or gluon jets lie in the region of phase space where they are experimentally identified as far-forward/backward tagging jets; and to estimate the additional QCD radiation patterns for the next-lower-order perturbative  $t\bar{t} + jets$  process. The  $t\bar{t}$  and  $t\bar{t}j$  matrix elements were constructed using MadGraph [19], while the  $t\bar{t}jj$  matrix elements are from Ref. [20].

Decays of the top quarks and  $W$ 's are included in the matrix elements; however, while the  $W$ 's are allowed to be off-shell, the top quarks are required to be on-shell. Energy loss from  $b \rightarrow \ell\nu X$  is included to generate more accurate  $\not{p}_T$  distributions. In all cases, the factorization scale is chosen as  $\mu_f = \min(E_T)$  of the massless partons/top quarks. The overall strong coupling constant factors are taken as  $(\alpha_s)^n = \prod_{i=1}^n \alpha_s(E_{T_i})$ , where the product runs over all light quarks, gluons and top quarks; *i.e.* the transverse momentum of each additional parton is taken as the relevant scale for its production, irrespective of the hardness of the underlying scattering event. This procedure guarantees that the same  $\alpha_s^2$  factors are used for the hard part of a  $t\bar{t} + jets$  event, independent of the number of additional minijets, and at the same time the small scales relevant for soft-parton emission are implemented.

### C. The QCD $WW + jj$ background

The next obvious background arises from real-emission QCD corrections to  $W^+W^-$  production. For  $W^+W^-jj$  events these background processes include [21]

$$gg \rightarrow qgW^+W^-, \quad qq' \rightarrow qq'W^+W^-, \quad (2)$$

which are dominated by  $t$ -channel gluon exchange, and all crossing related processes, such as

$$q\bar{q} \rightarrow ggW^+W^-, \quad gg \rightarrow q\bar{q}W^+W^-. \quad (3)$$

We call these processes collectively the “QCD  $WWjj$ ” background. We do not calculate cross sections for the corresponding  $WW + 3$ -jet processes, but instead follow the results of our analysis of the radiation patterns of QCD  $Z + jets$  processes, detailed in Sec. IV, and apply those results here to estimate minijet veto probabilities.

The factorization scale is chosen as for the Higgs boson signal. The strong coupling constant factor is taken as  $(\alpha_s)^2 = \alpha_s(p_{T_1})\alpha_s(p_{T_2})$ , *i.e.*, the transverse momentum of each additional parton is taken as the relevant scale for its production. Variation of the scales by a factor 2 or  $\frac{1}{2}$  reveals scale uncertainties of  $\approx 35\%$ , however, which emphasizes the need for experimental input or NLO calculations.

The  $WW$  background lacks the marked anti-correlation of  $W$  spins seen in the signal. As a result the momenta of the charged decay leptons will be more widely separated than in  $H \rightarrow W^{(*)}W^{(*)}$  events.

### D. The EW $WW + jj$ background

These backgrounds arise from  $W^+W^-$  bremsstrahlung in quark-(anti)quark scattering via  $t$ -channel electroweak boson exchange, with subsequent decay  $W^+W^- \rightarrow \ell^+\ell^-\not{p}_T$ :

$$qq' \rightarrow qq'W^+W^- \quad (4)$$

Naïvely, this EW background may be thought of as suppressed compared to the analogous QCD process in Eq. (2). However, it includes electroweak boson fusion,  $VV \rightarrow W^+W^-$  via  $s$ - or  $t$ -channel  $\gamma/Z$ -exchange or via  $VVVV$  4-point vertices, which has a momentum and color structure identical to the signal. Thus, it cannot easily be suppressed via cuts.

The matrix elements for these processes were constructed using MadGraph [19]. We include charged-current (CC) and neutral-current (NC) processes, but discard  $s$ -channel EW boson and  $t$ -channel quark exchange processes as their contribution was found to be  $\approx 1\%$  only, while adding significantly to the CPU time needed for the calculation. In general, for the regions of phase space containing far-forward and -backward tagging jets,  $s$ -channel processes are severely suppressed. We refer collectively to these processes as the “EW  $WWjj$ ” background. Both  $W$ ’s are allowed to be off-shell, and all off-resonance graphs are included. In addition, the Higgs boson graphs must be included to make the calculation well-behaved at large  $W$ -pair invariant masses. However, these graphs include our signal processes and might lead to double counting. Thus, we set  $m_H$  to 60 GeV in the EW  $WWjj$  background to remove their contribution. A clean separation of the Higgs boson signal and the EW  $WWjj$  background is possible because interference effects between the two are negligible for the Higgs boson mass range of interest.

Again we will need an estimate of additional gluon radiation patterns. This was first done for EW processes in Ref. [22], but for different cuts on the hard process, and again for EW  $\tau\tau jj$  processes in Ref. [17]. We reanalyze the EW  $\tau\tau jj$  case in Sec. IV and directly apply the resulting minijet emission probabilities here. The EW  $\tau\tau jj$  and EW  $WWjj$  backgrounds are quite similar kinematically, which justifies the use of the same veto probabilities for central jets.

### E. The QCD and EW $\tau^+\tau^-$ backgrounds

The leptonic decay of  $\tau$ ’s provides a source of electrons, muons and neutrinos which can be misidentified as  $W$  decays. Thus, we need to study real-emission QCD corrections to the Drell-Yan process  $q\bar{q} \rightarrow (Z, \gamma) \rightarrow \tau^+\tau^-$ . For  $\tau^+\tau^-jj$  events these background processes include [23]

$$qg \rightarrow qg\tau^+\tau^-, \quad qq' \rightarrow qq'\tau^+\tau^-, \quad (5)$$

which are dominated by  $t$ -channel gluon exchange, and all crossing-related processes, such as

$$q\bar{q} \rightarrow gg\tau^+\tau^-, \quad gg \rightarrow q\bar{q}\tau^+\tau^-. \quad (6)$$

All interference effects between virtual photon and  $Z$ -exchange are included. We call these processes collectively the “QCD  $\tau\tau jj$ ” background. The cross sections for the corresponding  $\tau\tau + 3$ -jet processes, which we need for our modeling of minijet activity in the QCD  $\tau\tau jj$  background, have been calculated in Refs. [24–26]. Similar to the treatment of the signal processes, we use a parton-level Monte-Carlo program based on the work of Ref. [25] to model the QCD  $\tau\tau jj$  and  $\tau\tau jjj$  backgrounds.

From our study of  $H \rightarrow \tau\tau$  in weak boson fusion [17], we know that the EW ( $t$ -channel weak boson exchange) cross section will be comparable to the QCD cross section in the phase space region of interest. Thus, we consider those processes separately, in a similar manner as for the EW  $WWjj$  contribution. We use the results of Ref. [27] for modeling the EW  $\tau\tau jj$  background.

The dual leptonic decays of the  $\tau$ ’s are simulated by multiplying the  $\tau^+\tau^-jj$  cross section by a branching ratio factor of  $(0.3518)^2/2$  and by implementing collinear tau decays with helicity correlations included as in our previous analysis of  $H \rightarrow \tau\tau$  [17].

### F. Detector resolution

The QCD processes discussed above lead to steeply falling jet transverse momentum distributions. As a result, finite detector resolution can have a sizable effect on cross sections. These resolution effects are taken into account via Gaussian smearing of the energies of jets/ $b$ ’s and charged leptons. We use

$$\frac{\Delta E}{E} = \frac{5.2}{E} \oplus \frac{0.4}{\sqrt{E}} \oplus .009, \quad (7)$$

for jets (with individual terms added in quadrature), based on ATLAS expectations [28]. For charged leptons we use

$$\frac{\Delta E}{E} = 2\% . \quad (8)$$

In addition, finite detector resolution leads to fake missing-transverse-momentum in events with hard jets. An ATLAS analysis [29] showed that these effects are well parameterized by a Gaussian distribution of the components of the fake missing transverse momentum vector,  $\vec{p}_T$ , with resolution

$$\sigma(p_x, p_y) = 0.46 \cdot \sqrt{\sum E_{T,had}} , \quad (9)$$

for each component. In our calculations, these fake missing transverse momentum vectors are added linearly to the neutrino momenta.

### III. HIGGS SIGNAL AND REAL $W^+W^-$ BACKGROUNDS

The  $qq \rightarrow qqH$ ,  $H \rightarrow W^{(*)}W^{(*)} \rightarrow e^\pm \mu^\mp \nu \bar{\nu}$  dual leptonic decay signal is characterized by two forward jets and the  $W$  decay leptons ( $e, \mu$ ). Before discussing background levels and further details like minijet radiation patterns, we need to identify the search region for these hard  $Hjj$  events. The task is identical to the Higgs searches in  $qq \rightarrow qqH$ ,  $H \rightarrow \gamma\gamma, \tau\tau$  which were considered previously [16,17]. We can thus adopt the strategy of these earlier analyses and start out by discussing a basic level of cuts on the  $qq \rightarrow qqH$ ,  $H \rightarrow W^{(*)}W^{(*)}$  signal. Throughout this section we assume a Higgs mass of  $M_H = 160$  GeV, but we do not optimize cuts for this mass.

The minimum acceptance requirements ensure that the two jets and two charged leptons are observed inside the detector (within the hadronic and electromagnetic calorimeters, respectively), and are well-separated from each other:

$$\begin{aligned} p_{T_j} &\geq 20 \text{ GeV}, & |\eta_j| &\leq 5.0, & \Delta R_{jj} &\geq 0.7, \\ p_{T_\ell} &\geq 20 \text{ GeV}, & |\eta_\ell| &\leq 2.5, & \Delta R_{j\ell} &\geq 0.7. \end{aligned} \quad (10)$$

A feature of the QCD  $WWjj$  background is the generally higher rapidity of the  $W$ 's as compared to the Higgs signal: weak boson bremsstrahlung occurs at small angles with respect to the parent quarks, producing  $W$ 's forward of the jets. Thus, we also require both  $\ell$ 's to lie between the jets with a separation in pseudorapidity  $\Delta\eta_{j,\ell} > 0.7$ , and the jets to occupy opposite hemispheres:

$$\eta_{j,min} + 0.7 < \eta_{\ell_{1,2}} < \eta_{j,max} - 0.7, \quad \eta_{j_1} \cdot \eta_{j_2} < 0 \quad (11)$$

Finally, to reach the starting point for our consideration of the signal and various backgrounds, a wide separation in pseudorapidity is required between the two forward tagging jets,

$$\Delta\eta_{tags} = |\eta_{j_1} - \eta_{j_2}| \geq 4.4, \quad (12)$$

leaving a gap of at least 3 units of pseudorapidity in which the  $\ell$ 's can be observed. This technique to separate weak boson scattering from various backgrounds is well-established [7–10,16–18], in particular for heavy Higgs boson searches. Line 1 of Table I shows the effect of these cuts on the signal and backgrounds for a SM Higgs boson of mass  $m_H = 160$  GeV. Overall, about 28% of all  $H \rightarrow W^{(*)}W^{(*)} \rightarrow e^\pm \mu^\mp \nu \bar{\nu}$  events generated in weak boson fusion are accepted by the cuts of Eqs. (10–12) (for  $m_H = 160$  GeV).

Somewhat surprisingly, the EW  $WWjj$  background rate reaches 2/3 of the QCD  $WWjj$  background rate already at this level. This can be explained by the contribution from  $W, Z, \gamma$  exchange and fusion processes which can produce central  $W$  pairs and are therefore kinematically similar to the signal. This signal-like component remains after the forward jet tagging cuts.

As is readily seen from the first line of Table I, the most worrisome background is  $W$  pairs from  $t\bar{t} + jets$  production. Of the 1080 fb at the basic cuts level, 12 fb are from  $t\bar{t}$ , 310 fb are from  $t\bar{t}j$ , and the remaining 760 fb arise from  $t\bar{t}jj$  production. The additional jets (corresponding to massless partons) are required to be identified as far forward tagging jets. The  $t\bar{t}jj$  cross section is largest because the  $t\bar{t}$  pair is not required to have as large an invariant mass as in the first two cases, where one or both  $b$ 's from the decay of the top quarks are required to be the tagging jets.

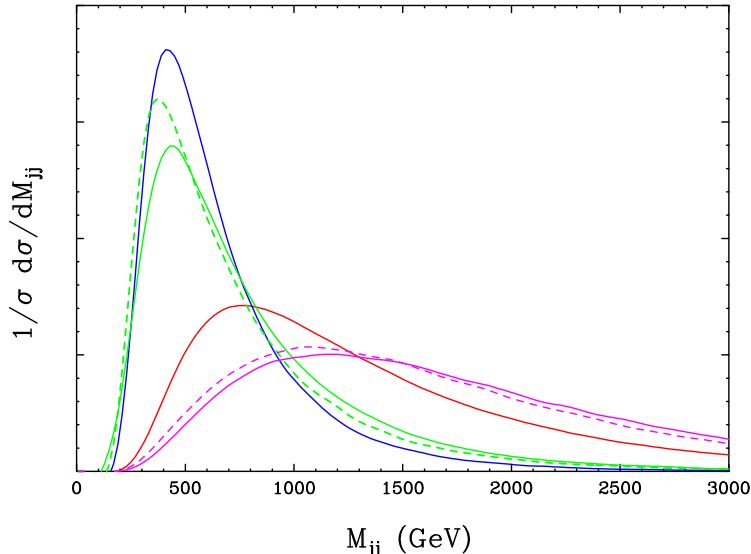


FIG. 1. Normalized invariant mass distribution of the two tagging jets for the signal (red) and various backgrounds:  $t\bar{t} + jets$  (blue), QCD  $WWjj$  (solid green), EW  $WWjj$  (solid purple), QCD  $\tau\tau + jj$  (dashed green) and EW  $\tau\tau + jj$  (dashed purple). The cuts of Eqs. (10-13) are imposed.

For the events where one or both of the  $b$ 's are not identified as the tagging jets, they will most frequently lie between the two tagging jets, in the region where we search for the  $W$  decay leptons. Vetoing events with these additional  $b$  jets provides a powerful suppression tool to control the top background. Note that this does *not* require a  $b$ -tag, merely rejection of any events that have an additional jet, which in this case would be from a hadronically decaying  $b$ . We discard all events where a  $b$  or  $\bar{b}$  jet with  $p_T > 20$  GeV is observed in the gap region between the tagging jets,

$$p_{T_b} > 20\text{GeV}, \quad \eta_{j,min} < \eta_b < \eta_{j,max}. \quad (13)$$

This leads to a reduction of  $t\bar{t}j$  events by a factor 7 while  $t\bar{t}jj$  events are suppressed by a factor 100. This results in cross sections of 43 and 7.6 fb, respectively, at the level of the forward tagging cuts of Eqs. (10-12), which are now comparable to the other individual backgrounds. This is shown in the second line of Table I. Note that the much higher  $b$  veto probability for  $t\bar{t}jj$  events results in a lower cross section than that for  $t\bar{t}j$  events, an ordering which will remain even after final cuts have been imposed (see below).

QCD processes at hadron colliders typically occur at smaller invariant masses than EW processes, due to the dominance of gluons at small Feynman  $x$  in the incoming protons. We observe this behavior here, as shown in Fig. 1. The three  $t\bar{t} + jets$  backgrounds have been combined for clarity, even though their individual distributions are slightly different. We can thus significantly reduce much of the QCD background by imposing a lower bound on the invariant mass of the tagging jets:

$$m_{jj} > 650 \text{ GeV}. \quad (14)$$

Another significant difference is the angular distribution of the charged decay leptons,  $e^\pm$  and  $\mu^\mp$ , relative to each other. In the case of the Higgs signal, the  $W$  spins are anti-correlated, so the leptons are preferentially emitted in the same direction, close to each other. A significant fraction of the various backgrounds does not have anti-correlated  $W$  spins. These differences are demonstrated in Fig. 2, which shows the azimuthal (transverse plane) opening angle, polar (lab) opening angle, and separation in the lego plot. We exploit these features by establishing the following lepton-pair angular cuts:

$$\phi_{e\mu} < 105^\circ, \quad \cos \theta_{e\mu} > 0.2, \quad \Delta R_{e\mu} < 2.2. \quad (15)$$

It should be noted that while these cuts appear to be very conservative, for higher Higgs boson masses the  $\phi_{e\mu}$  and  $\Delta R_{e\mu}$  distribution broadens out to higher values, overlapping the backgrounds more. For  $m_H \sim 180 - 200$  GeV these cuts are roughly optimized and further tightening would require greater integrated luminosity for discovery

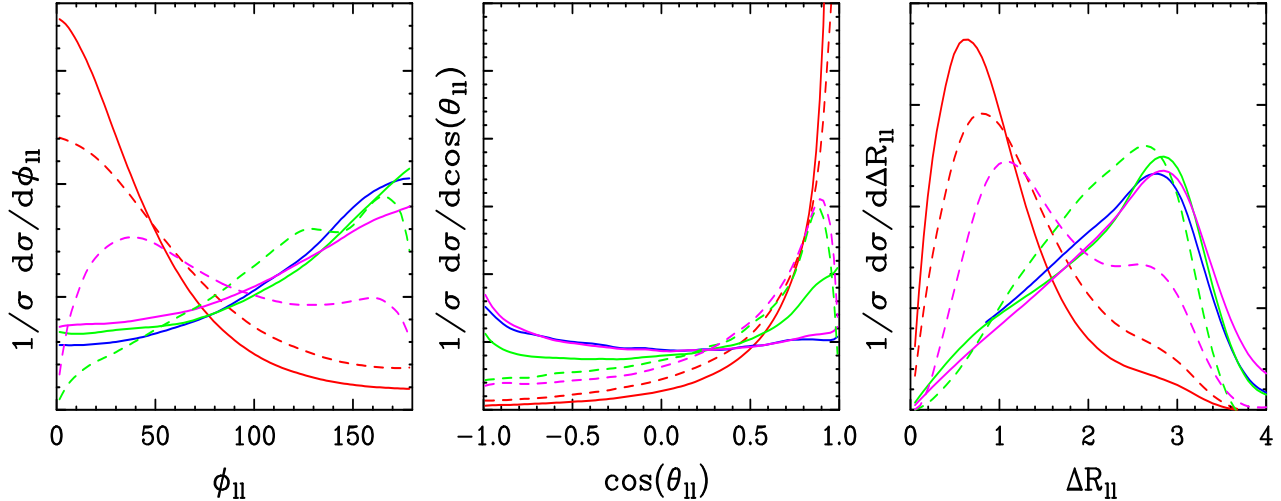


FIG. 2. Normalized angular distributions of the charged leptons: azimuthal opening angle, lab opening angle, and separation in the lego plot. Results are shown for a Higgs boson mass of 160 GeV and 190 GeV (solid and dashed red lines) and for the various backgrounds as in Fig. 1. Lepton angular separation is clearly smaller for the  $m_H = 160$  GeV scenario. The cuts of Eqs. (10-13) are imposed.

TABLE I. Signal rates  $\sigma \cdot B(H \rightarrow e^\pm \mu^\mp \not{p}_T)$  for  $m_H = 160$  GeV and corresponding background cross sections, in  $pp$  collisions at  $\sqrt{s} = 14$  TeV. Results are given for various levels of cuts and are labeled by equation numbers discussed in the text. On lines six the minijet veto is included. Line five gives the survival probabilities for each process, with  $p_T^{\text{veto}} = 20$  GeV. The expected tagging jet identification efficiency is shown on the last line. All rates are given in fb.

cuts	$Hjj$	$t\bar{t} + jets$	QCD $WWjj$	EW $WWjj$	QCD $\tau\tau jj$	EW $\tau\tau jj$	S/B
forward tagging (10-12)	17.1	1080	4.4	3.0	15.8	0.8	$\approx 1/65$
+ $b$ veto (13)		64					1/5.1
+ $M_{jj}$ , angular cuts (14-16)	11.8	5.5	0.54	0.50	3.6	0.4	1.1/1
+ real $\tau$ rejection (17)	11.4	5.1	0.50	0.45	0.6	0.08	1.7/1
$P_{\text{surv},20}$	$\times 0.89$	$\times 0.29$	$\times 0.29$	$\times 0.75$	$\times 0.29$	$\times 0.75$	-
+ minijet veto (18)	10.1	1.48	0.15	0.34	0.18	0.07	4.6/1
+ tag ID efficiency ( $\times 0.74$ )	7.5	1.09	0.11	0.25	0.13	0.05	4.6/1

at this upper end of the mass range. Because of the excellent signal-to-background ratio achieved below, we prefer to work with uniform acceptance cuts, instead of optimizing the cuts for specific Higgs boson mass regions.

We also examine the distributions for lepton-pair invariant mass,  $m_{e\mu}$ , and maximum lepton  $p_T$ , as shown in Fig. 3 for the case  $m_H = 160, 190$  GeV. As is readily seen, the QCD backgrounds and EW  $WWjj$  background prefer significantly higher values for both observables. Thus, in addition to the angular variables, we find it useful to restrict the individual  $p_T$  of the leptons, as well as the invariant mass of the pair:

$$m_{e\mu} < 110 \text{ GeV}, \quad p_{T_{e,\mu}} < 120 \text{ GeV}. \quad (16)$$

These are particularly effective against the top backgrounds, where the large top mass allows for very high- $p_T$  leptons far from the tagging jets, and against the EW  $WWjj$  background, where the leptons tend to be well-separated in the lego plot. Again, the cuts are set quite conservatively so as not to bias a lower Higgs boson mass. Results after cuts (14-16) are shown on the third line of Table I, for the case of a 160 GeV Higgs boson.

At this level of cuts we now observe the combined QCD and EW  $\tau\tau jj$  backgrounds to remain large, contributing almost 40% of the total. We can take advantage of the fact that in these backgrounds, the  $Z$  or  $\gamma$  is emitted with quite high  $p_T$ , on the order of 100 GeV, which contributes to large  $\tau$  boosts and causes the  $\tau$  decay products to be nearly collinear in the lab frame. Within the collinear approximation, the  $\tau$  momenta can be reconstructed knowing the charged lepton momenta and the missing transverse momentum vector [17,29]. Labeling by  $x_{\tau_1}, x_{\tau_2}$  the fraction of  $\tau$  energy each charged lepton takes with it in the  $\tau$  decay,  $\not{p}_{T,x}, \not{p}_{T,y}$  can be used to solve the two

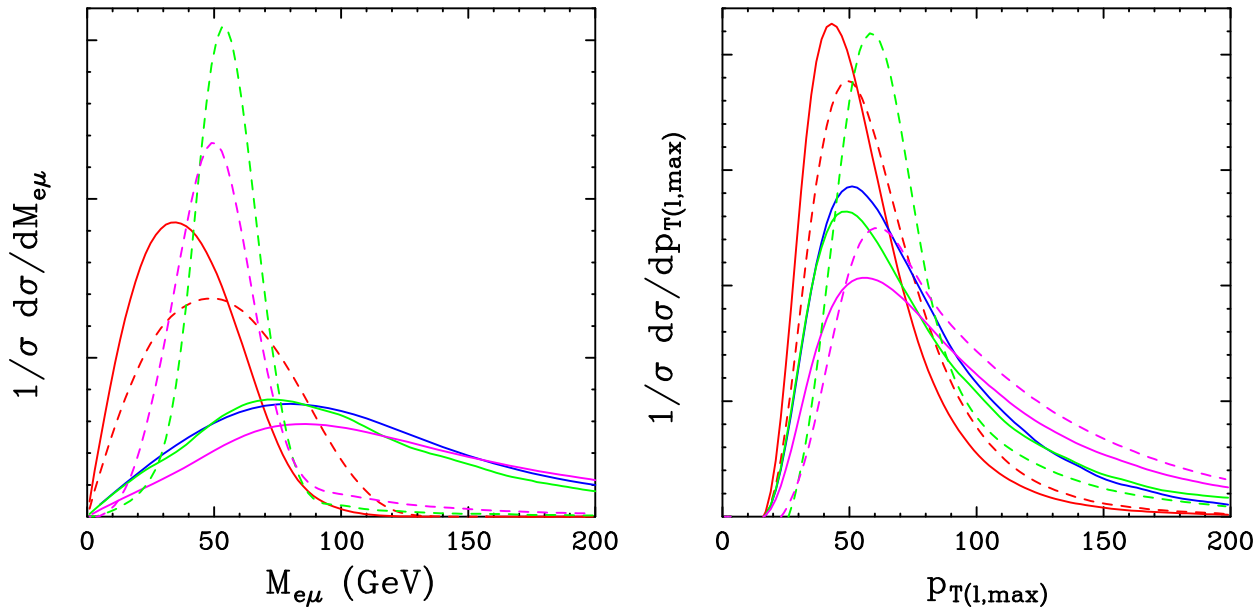


FIG. 3. Normalized distributions of the dilepton invariant mass and maximum charged lepton momentum after the cuts of Eqs. (10-13). Results are shown for a Higgs boson mass of 160 GeV and 190 GeV (solid and dashed red lines) and for the various backgrounds as in Fig. 1. The  $m_H = 160$  GeV curve peaks at lower values of  $m_{e\mu}$  and  $p_{T,\max}$ .

equations ( $x, y$  transverse directions) for the two unknowns  $x_{\tau_{1,2}}$ . For real  $\tau$  decays, the  $\not{p}_T$  vector must lie between the two leptons, and apart from finite detector resolution the reconstruction must yield  $0 < x_{\tau_{1,2}} < 1$ . For the  $Hjj$  signal and other backgrounds, the collinear approximation is not valid because the  $W$ 's receive modest boosts in the lab only. In this case, the  $\not{p}_T$  vector will rarely lie between the two leptons, and an attempt to reconstruct a  $\tau$  pair will result in  $x_{\tau_1} < 0$  or  $x_{\tau_2} < 0$  for 95% of the events.<sup>1</sup> Additionally, the “ $\tau$  pair” invariant mass that is reconstructed does not peak at  $m_Z$ , even when it is positive. We can therefore apply a highly efficient cut against the QCD and EW  $\tau\tau jj$  backgrounds by vetoing events where an attempt to reconstruct a  $\tau$  pair in the collinear decay approximation results in two “real”  $\tau$ 's near the  $Z$  pole:

$$x_{\tau_1}, x_{\tau_2} > 0, \quad m_Z - 25 \text{ GeV} < m_{\tau\tau} < m_Z + 25 \text{ GeV}. \quad (17)$$

The results of this final cut are shown in line four of Table I. The  $\tau$  backgrounds are virtually eliminated, while the signal and the other backgrounds each lose  $\approx 5\%$ .

#### IV. RADIATION PATTERNS OF MINIJETS

If we are to veto central  $b$  jets to reduce the  $t\bar{t} + jets$  background to a manageable level, we must take care to correctly estimate higher-order additional central partonic emission in the signal and backgrounds. Fortunately, due to the absence of color exchange between the two scattering quarks in EW processes, which includes our  $Hjj$  signal, we expect soft gluon emission mainly in the very forward and very backward directions. However, for QCD processes, which are dominated by  $t$ -channel color octet exchange, soft gluon radiation occurs mainly in the central detector. Thus, when we estimate additional central radiation with  $p_T \geq 20$  GeV to match our  $b$  veto condition, we will reject QCD background events with much higher probability than the EW processes. Our  $b$  veto is then automatically also a minijet veto, a tool for QCD background suppression which has been previously studied in great detail for  $Hjj$  production at hadron colliders [7,17,22].

<sup>1</sup>Conversely, requiring  $x_{\tau_1} > 0, x_{\tau_2} > 0$  largely eliminates  $WW$  backgrounds and promises clean isolation of  $H \rightarrow \tau\tau \rightarrow e^\pm \mu^\mp \not{p}_T$  [30].



Largely following the analysis of Ref. [18] for the analogous EW  $Zjj$  process which would be used to “calibrate” the tool at the LHC, we veto additional central jets in the region

$$p_{Tj}^{\text{veto}} > p_{T,\text{veto}} , \quad (18a)$$

$$\eta_{j,\text{min}}^{\text{tag}} < \eta_j^{\text{veto}} < \eta_{j,\text{max}}^{\text{tag}} , \quad (18b)$$

where  $p_{T,\text{veto}}$  may be chosen based on the capability of the detector. For the LHC we take this to be 20 GeV.

For  $p_{T,\text{veto}} \approx 40$  GeV we are already leaving the validity range of fixed-order perturbation theory in QCD processes: the cross section with one additional parton starts to exceed the hard tree-level cross section. As a result it becomes difficult to provide reliable theoretical estimates of minijet emission rates for the QCD backgrounds. However, gluon emission is governed by very different scales in signal as compared to background processes, due to their different color structures. Thus, a parton shower approach does not immediately give reliable answers unless both color coherence and the choice of scale are implemented correctly, matching the answer given by QCD matrix elements for sufficiently hard partons.

While the necessary information on angular distributions and hardness of additional radiation is available in the “3-jet” and  $t\bar{t} + jets$  processes discussed in Section II, we must either regulate or reinterpret these divergent cross sections. We use the truncated shower approximation (TSA) [12] for the former, treating the “2-jet” cross sections as the inclusive rate. Details of this procedure can be found in Refs. [17,18], but here we improve upon the determination of veto probabilities. In our previous studies, TSA matching was performed without enforcement of the forward tagging cuts of Eqs. (11,12), even though tagging jet candidates were chosen for the purpose of identifying the veto candidate; tagging jet candidates were selected as the two most energetic [18] or two highest- $p_T$  [17] defined jets ( $p_T > 20$  GeV), in opposite detector hemispheres. Without the additional forward tagging cuts, in particular without the large rapidity separation of the two tagging jets, this favors QCD background events with high  $p_T$  central quark jets which in turn lead to a harder gluon emission spectrum than is present after all final cuts are imposed. A harder gluon spectrum goes hand-in-hand, however, with an increased minijet emission probability. A more realistic estimate of the minijet  $p_T$  spectrum is obtained by applying the matching condition (or calculating  $\bar{n}$ ) only in the phase space region where a comparison of signal and background will take place: after all acceptance cuts, determined at the two-jet level, have been imposed.

Once the full level of cuts for a given search scenario are imposed, one may examine different tagging jet selection algorithms to optimize the veto. Ideally, the outgoing quarks would always be selected, so that the additional gluon radiation is always the veto candidate. In practice, this is impossible, but for the Higgs signal various algorithms can achieve “proper” quark tagging with about 75% efficiency, a high success rate. Briefly, these might be the two highest- $p_T$  jets, or the two jets closest to the reconstructed Higgs. Most algorithms have very little difference from each other in the case of the WBF signature. Thus, we choose an algorithm that allows more suppression of the QCD backgrounds. The final algorithm we chose is to select the highest- $p_T$  jet as the first tagging jet, since it will almost always be part of the hard scattering, and then select the other tagging jet such that the event is more likely to pass the forward tagging cuts: look for jets with  $p_T > 20$  GeV in the opposite hemisphere, such that the candidate Higgs decay products are between the tagging jets, satisfying Eq. (11). This performs somewhat superior to merely choosing the two highest- $p_T$  jets.

Also in contrast to our previous studies [17,18], the veto candidates are defined jets ( $p_T > 20$  GeV) anywhere between the tagging jets, *i.e.* they are searched for in a somewhat larger rapidity region than the  $W$  decay leptons (see Eq. (11), which have to be at least 0.7 units of rapidity away from the tagging jets. The choice of Eq. (18b) allows for more suppression of the backgrounds than the more restrictive selection. The resulting veto probabilities are summarized in line six of Table I. We emphasize that while these probabilities are estimates only, they can be independently determined at the LHC in processes like  $Zjj$  and  $Wjj$  production [18,27].

For the  $t\bar{t} + jets$  backgrounds, it is simpler instead to reinterpret the divergent higher-order cross sections. For this we assume that additional soft parton emission, which will be dominated by soft gluons, exponentiates like soft photon emission. This approximation has been shown well to describe multijet events at the Tevatron [13]. In this model, the probability to observe  $n$  soft jets in the veto region is given by a Poisson distribution with

$$\bar{n} = \bar{n}(p_{T,\text{veto}}) = \frac{1}{\sigma_2} \int_{p_{T,\text{veto}}}^{\infty} dp_{T3} \frac{d\sigma_3}{dp_{T3}} , \quad (19)$$

where the unregularized three-parton cross section is integrated over the veto region of Eq. (18) and then normalized to the 2-jet cross section  $\sigma_2$ , regarded as inclusive. We call this model the “exponentiation model”. A rough estimate of the multiple emission probability is thus provided by

$$P_{exp}(p_{T,\text{veto}}) = 1 - P_0 = 1 - e^{-\bar{n}(p_{T,\text{veto}})} \quad (20)$$

TABLE II. Number of expected events for the  $Hjj$  signal, for  $5 \text{ fb}^{-1}$  integrated luminosity and application of all efficiency factors and cuts, including a minijet veto, but for a range of Higgs boson masses. The total background is 8.1 events. As a measure of the Poisson probability of the background to fluctuate up to the signal level, the second line gives  $\sigma_{Gauss}$ , the number of Gaussian equivalent standard deviations.

$m_H$	115	120	130	140	150	160	170	180	190	200
no. events	2.0	3.6	8.8	15.8	24.0	37.5	36.3	29.9	20.8	16.3
$\sigma_{Gauss}$	0.5	1.0	2.6	4.4	6.3	9.0	8.8	7.5	5.5	4.5

which is the probability to veto the event. We find veto survival probabilities of  $P_{surv} = 46\%$  for  $t\bar{t}$  events and  $P_{surv} = 12\%$  for  $t\bar{t}j$  events. Both of these results disagree with our other estimates of  $P_{surv}$  for QCD processes. This may be understandable for  $t\bar{t}$  events, as at tree level this component does not contain any t-channel gluon exchange processes, which all of the other QCD backgrounds do. We also observe that the additional radiation in  $t\bar{t}$  events typically falls outside the central gap. We did not explore this any further as the  $t\bar{t}$  component is negligible. That the value of  $P_{surv}$  found for  $t\bar{t}j$  events is so much smaller than that for other QCD backgrounds may be understood because the large mass of the tops produced requires significant  $p_T$ , but as this is not yet fully explored we prefer to remain conservative and assume the value  $P_{surv} = 0.29$  for all QCD backgrounds, including top quark pair production. For a Higgs boson mass of 160 GeV we are left with a signal cross section of 7.5 fb compared to a total background of 1.6 fb.

So far we have considered a single Higgs boson mass of 160 GeV only. Since we have largely avoided mass-specific cuts, we can immediately extend our results to a larger range of  $m_H$ . The expected number of signal events for  $115 \text{ GeV} \leq m_H \leq 200 \text{ GeV}$  and an integrated luminosity of  $5 \text{ fb}^{-1}$  are shown in Table II. For the same luminosity, 8.1 background events are expected. In the second row of Table II the Poisson probabilities for this background to fluctuate up to the signal level are given, in terms of the equivalent Gaussian significances which can be expected in the experiment on average.

## V. DISCUSSION

While we have demonstrated a series of kinematic cuts and a minijet veto, based on the physics of the processes involved, that reduce the background well below the level of the signal, we have not performed a detailed detector simulation. A full simulation is clearly needed eventually, but we do not expect our results to change dramatically since CMS and ATLAS will be highly efficient detectors. For a more realistic estimate of the signal significance we do take one major reduction factor into account in the last line of Table I, the reconstruction efficiency for tagging jets. This is expected to be 0.86 at CMS for each tagging jet, resulting in a net efficiency of  $\epsilon_{tag} = (0.86)^2 = 0.74$ . Even after this nontrivial loss of total rate, it is clear that the method we propose still works beautifully.

As the  $H \rightarrow WW$  mode is likely to be the discovery channel for the mass range  $130 \text{ GeV} < m_H < 200 \text{ GeV}$ , we wish to be able to reconstruct the Higgs boson mass. At threshold, the two (virtual)  $W$ 's are at rest in the Higgs boson center-of-mass frame, resulting in  $m_{e\mu} = m_{\nu\bar{\nu}}$ , so we can calculate the transverse energy of both the charged lepton and invisible neutrino systems,

$$E_{T_{e\mu}} = \sqrt{\vec{p}_{T_{e\mu}}^2 + m_{e\mu}^2}, \quad E_T = \sqrt{\vec{p}_T^2 + m_{e\mu}^2}. \quad (21)$$

Using these results for the transverse energies, we may compute a transverse mass of the dilepton- $\vec{p}_T$  system,

$$M_{T_{WW}} = \sqrt{(E_T + E_{T_{e\mu}})^2 - (\vec{p}_{T_{e\mu}} + \vec{p}_T)^2}, \quad (22)$$

At threshold this is exactly the Higgs boson transverse mass. Below threshold, the relation  $m_{e\mu} = m_{\nu\bar{\nu}}$  is still an excellent approximation, while above threshold it begins to lose validity as the  $W$  bosons acquire a non-zero velocity in the Higgs boson rest frame. But even at  $m_H = 200 \text{ GeV}$  this ‘‘pseudo’’ transverse mass remains extremely useful for mass reconstruction. We show the dramatic results in Fig. 4, for Higgs boson masses of 130, 160 and 190 GeV. Clearly visible is the Jacobian peak at  $M_{T_{WW}} = m_H$ , in particular for  $m_H = 160 \text{ GeV}$ . The combined backgrounds are added to the Higgs signal, and are shown after application of all cuts and detector efficiencies, as well as both the  $b$  and minijet vetoes which were discussed in the previous Sections.

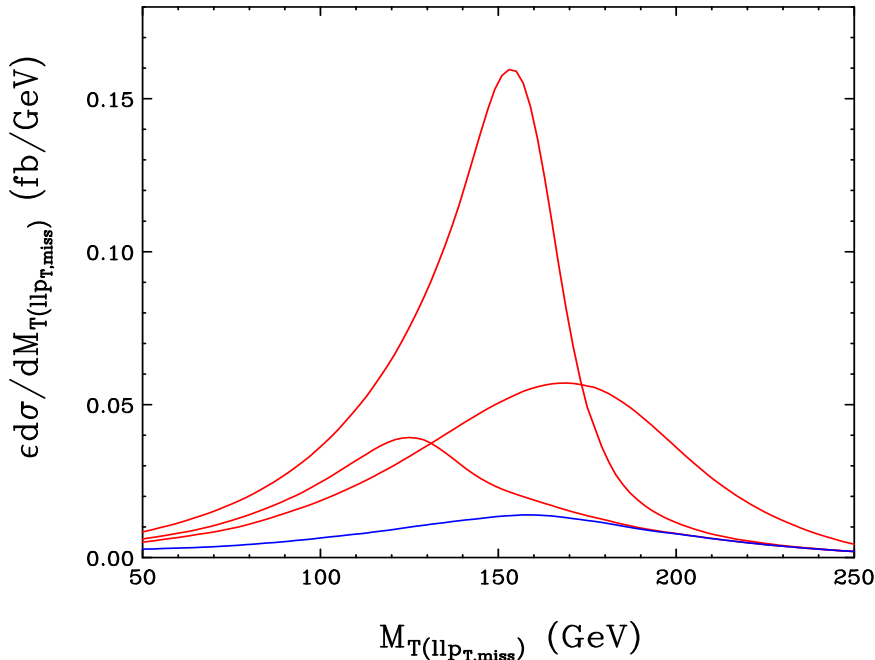


FIG. 4. Dilepton- $p_T$  transverse mass distributions expected for a Higgs boson of mass  $m_H = 130, 160,$  and  $190$  GeV (red) after the cuts of Eqs. (10-16) and application of all detector efficiencies and a minijet veto with  $p_{T,\text{veto}} = 20$  GeV. Also shown is the background only (dashed).

As the  $M_T$  distribution shows a pronounced Jacobian peak for all Higgs boson masses under consideration, the signal-to-background ratio and the statistical significance of the signal can be improved by restricting attention to the relevant  $M_T$  range. We find that up to  $W$ -pair threshold ( $M_H \leq 165$  GeV), the requirement  $M_T < M_H + 20$  GeV works well. Above threshold, loosening this cut improves the signal significance. Table III demonstrates the power of this constraint, showing that it is possible to isolate a virtually background free  $qq \rightarrow qqH$ ,  $H \rightarrow WW$  signal at the LHC, with sufficiently large counting rate to obtain a better than  $5\sigma$  signal with a mere  $5 \text{ fb}^{-1}$  of data for the mass range 140-200 GeV. Extending the observability region down to 130 GeV requires at most  $15 \text{ fb}^{-1}$ . To reach 120 GeV would require  $\approx 65 \text{ fb}^{-1}$  of low luminosity data ( $10^{33} \text{ cm}^{-2} \text{ s}^{-1}$ ), and to reach 115 GeV would require  $\approx 165 \text{ fb}^{-1}$ . This nicely overlaps the regions of observability for  $H \rightarrow \gamma\gamma$  (100-150 GeV) [16] and  $H \rightarrow \tau\tau$  (110-140 GeV) [17]. The luminosity requirements in the low mass region can be reduced significantly by more stringent charged lepton cuts.

The high purity of the signal is made possible because the weak boson fusion process, together with the  $H \rightarrow W^+W^- \rightarrow e^\pm\mu^\mp p_T$  decay, provides a complex signal with a multitude of characteristics which distinguish

TABLE III. Number of expected events for the  $Hjj$  signal, for  $5 \text{ fb}^{-1}$  integrated luminosity and a range of Higgs masses. As compared to Table II an additional upper limit on the Higgs transverse mass of Eq. (22) is imposed, as given in the first line. The number of both signal and background events are shown, as well as S/B. The Poisson probability of the background to fluctuate up to the signal level is given in terms of  $\sigma_{Gauss}$ , the number of Gaussian equivalent standard deviations.

$m_H$ (GeV)	115	120	130	140	150	160	170	180	190	200
$M_T$ cutoff (GeV)	135	140	150	160	170	180	210	220	none	none
no. S events	1.9	3.4	8.3	14.8	22.7	36.5	35.9	29.3	20.8	16.3
no. B events	3.0	3.4	4.0	4.7	5.4	6.0	7.2	7.5	8.1	8.1
S/B	0.6	1.0	2.0	3.1	4.2	6.1	5.0	3.9	2.6	2.0
$\sigma_{Gauss}$	0.8	1.4	3.1	5.0	6.8	9.6	9.0	7.6	5.5	4.5

it from the various backgrounds. The basic feature of the  $qq \rightarrow qqH$  signal is the presence of two forward tagging jets inside the acceptance region of the LHC detectors, of sizable  $p_T$ , and of dijet invariant mass in the TeV range. Typical QCD backgrounds, with isolated charged leptons and two hard jets, are much softer. In addition, the QCD backgrounds are dominated by  $W$  bremsstrahlung off forward scattered quarks, which give typically higher-rapidity charged leptons. In contrast, the EW processes give rise to quite central leptons, and this includes not only the Higgs signal but also EW  $WWjj$  and  $\tau\tau jj$  production, which also proceed via weak boson fusion. It is this similarity that prevents one from ignoring EW analogs to background QCD processes, which a priori are smaller by two orders of magnitude in total cross section, but after basic cuts remain the same size as their QCD counterparts.

For  $H \rightarrow WW$  decays, lepton angular distributions are extremely useful for reducing the backgrounds even further. The anti-correlation of  $W$  spins in  $H$  decay forces the charged leptons to be preferentially emitted in the same direction, close together in the lego plot. This happens for a small fraction of the background only. We have identified the most important distributions for enhancing the signal relative to the background, and set the various cuts conservatively to avoid bias for a certain Higgs boson mass range. There is ample room for improvement of our results via a multivariate analysis of a complete set of signal and background distributions, which we encourage the LHC collaborations to pursue. Additional suppression of the  $t\bar{t} + jets$  background may be possible with  $b$  identification and veto in the  $p_{T_b} < 20$  GeV region.

In addition to various invariant mass and angular cuts, we can differentiate between the  $W$ 's of the signal and  $W, t$  backgrounds and the real  $\tau$ 's in the QCD and EW  $\tau\tau jj$  backgrounds. This is possible because the high energy of the produced  $\tau$ 's makes their decay products almost collinear. Combined with the substantial  $p_T$  of the  $\tau^+\tau^-$  system this allows for  $\tau$ -pair mass reconstruction. The  $W$  decays do not exhibit this collinearity due to their large mass, thus the angular correlation between the  $\not{p}_T$  vector and the charged lepton momenta is markedly different. Our real- $\tau$  rejection makes use of these differences and promises to virtually eliminate the  $\tau\tau jj$  backgrounds.

We advocate taking advantage of an additional fundamental characteristic of QCD and EW processes. Color-singlet exchange in the  $t$ -channel, as encountered in Higgs boson production by weak boson fusion (and in the EW  $Zjj$  background), leads to additional soft jet activity which differs strikingly from that expected for the QCD backgrounds in both geometry and hardness: gluon radiation in QCD processes is typically both more central and harder than in WBF processes. We exploit this radiation, via a veto on events with central minijets of  $p_T > 20$  GeV, and expect a typical 70% reduction in QCD backgrounds and about a 25% suppression of EW backgrounds, but only about a 10% loss of the signal.

Beyond the possibility of discovering the Higgs boson in the  $H \rightarrow WW$  mode, or confirmation of its existence, measuring the cross sections in both weak boson and gluon fusion will be important both as a test of the Standard Model and as a search for new physics. For such a measurement, via the analysis outlined in this paper, minijet veto probabilities must be precisely known. For calibration purposes, one can analyze  $Zjj$  events at the LHC. The production rates of the QCD and EW  $Zjj$  events can be reliably predicted and, thus, the observation of the  $Z \rightarrow \ell\ell$  peak allows for a direct experimental assessment of the minijet veto efficiencies, in a kinematic configuration very similar to the Higgs signal.

Observation of SM  $H \rightarrow e^\pm\mu^\mp\not{p}_T$  at the LHC is possible for very low integrated luminosities, if the Higgs boson lies in the mass range between about 130 and 200 GeV. Weak boson fusion at the LHC will be an exciting process to study, for a weakly coupled Higgs sector just as much as for strong interactions in the symmetry breaking sector of electroweak interactions.

## ACKNOWLEDGMENTS

This research was supported in part by the University of Wisconsin Research Committee with funds granted by the Wisconsin Alumni Research Foundation and in part by the U. S. Department of Energy under Contract No. DE-FG02-95ER40896.

- 
- [1] For recent reviews, see e.g. J.L. Rosner, Comments Nucl. Part. Phys. **22**, 205 (1998) [hep-ph/9704331]; K.Hagiwara, Ann. Rev. Nucl. Part. Sci. 1998, 463; W.J. Marciano, hep-ph/9902332; and references therein.
- [2] For recent reviews, see e.g. S. Dawson, [hep-ph/9703387]; M. Spira, Fortsch. Phys. **46**, 203 (1998); and references therein.
- [3] W. J. Marciano and F. E. Paige, Phys. Rev. Lett. **66**, 2433 (1991); J. F. Gunion, Phys. Lett. **B261**, 510 (1991).
- [4] A. Stange, W. Marciano, and S. Willenbrock, Phys. Rev. **D50**, 4491 (1994), [hep-ph/9404247]; R. Kleiss, Z. Kunszt, W. J. Stirling, Phys. Lett. **B253**, 269 (1991); H. Baer, B. Bailey, J. F. Owens, Phys. Rev. **D47**, 2730 (1993).
- [5] E.W. Glover, J. Ohnemus and S.S. Willenbrock, Phys. Rev. **D37**, 3193 (1988); V. Barger, G. Bhattacharya, T. Han and B.A. Kniehl, Phys. Rev. **D43**, 779 (1991).
- [6] M. Dittmar and H. Dreiner, Phys. Rev. **D55**, 167 (1997); and [hep-ph/9703401].
- [7] V. Barger, R. J. N. Phillips, and D. Zeppenfeld, Phys. Lett. **B346**, 106 (1995).
- [8] R. N. Cahn, S.D. Ellis, R. Kleiss and W.J. Stirling, Phys. Rev. **D35**, 1626 (1987); V. Barger, T. Han, and R. J. N. Phillips, Phys. Rev. **D37**, 2005 (1988); R. Kleiss and W. J. Stirling, Phys. Lett. **200B**, 193 (1988); D. Froideveaux, in *Proceedings of the ECFA Large Hadron Collider Workshop*, Aachen, Germany, 1990, edited by G. Jarlskog and D. Rein (CERN report 90-10, Geneva, Switzerland, 1990), Vol II, p. 444; M. H. Seymour, *ibid*, p. 557; U. Baur and E. W. N. Glover, Nucl. Phys. **B347**, 12 (1990); Phys. Lett. **B252**, 683 (1990).
- [9] V. Barger, K. Cheung, T. Han, and R. J. N. Phillips, Phys. Rev. **D42**, 3052 (1990); V. Barger *et al.*, Phys. Rev. **D44**, 1426 (1991); V. Barger, K. Cheung, T. Han, and D. Zeppenfeld, Phys. Rev. **D44**, 2701 (1991); erratum Phys. Rev. **D48**, 5444 (1993); Phys. Rev. **D48**, 5433 (1993); V. Barger *et al.*, Phys. Rev. **D46**, 2028 (1992).
- [10] D. Dicus, J. F. Gunion, and R. Vega, Phys. Lett. **B258**, 475 (1991); D. Dicus, J. F. Gunion, L. H. Orr, and R. Vega, Nucl. Phys. **B377**, 31 (1991).
- [11] Y. L. Dokshitzer, V. A. Khoze, and S. Troian, in *Proceedings of the 6th International Conference on Physics in Collisions*, (1986) ed. M. Derrick (World Scientific, 1987) p.365; J. D. Bjorken, Int. J. Mod. Phys. **A7**, 4189 (1992); Phys. Rev. **D47**, 101 (1993).
- [12] V. Barger and R. J. N. Phillips, Phys. Rev. Lett. **55**, 2752 (1985); H. Baer, V. Barger, H. Goldberg, and R. J. N. Phillips, Phys. Rev. **D37**, 3152 (1988).
- [13] D. Rainwater, D. Summers, and D. Zeppenfeld, Phys. Rev. **D55**, 5681 (1997).
- [14] H. L. Lai *et al.*, Phys. Rev. **D55**, 1280 (1997), [hep-ph/9606399].
- [15] R. Cahn and S. Dawson, Phys. Lett. **136B**, 196 (1984).
- [16] D. Rainwater and D. Zeppenfeld, Journal of High Energy Physics 12, 005 (1997).
- [17] D. Rainwater, D. Zeppenfeld and K. Hagiwara, Phys. Rev. **D59**, 014037 (1999).
- [18] D. Rainwater, R. Szalapski, and D. Zeppenfeld, Phys. Rev. **D54**, 6680 (1996), [hep-ph/9605444].
- [19] T. Stelzer and W. F. Long, Comp. Phys. Comm. **81**, 357 (1994), [hep-ph/9401258].
- [20] A. Stange, private communication.
- [21] V. Barger, T. Han, J. Ohnemus and D. Zeppenfeld, Phys. Rev. **D41**, 2782 (1990).
- [22] A. Duff and D. Zeppenfeld, Phys. Rev. **D50**, 3204 (1994); K. Iordanidis and D. Zeppenfeld, Phys. Rev. **D57**, 3072 (1998), [hep-ph/9709506].
- [23] S. D. Ellis, R. Kleiss, and W. J. Stirling, Phys. Lett. **154B**, 435 (1985); R. Kleiss and W. J. Stirling, Nucl. Phys. **B262**, 235 (1985); Phys. Lett. **180B**, 171 (1986); J. F. Gunion, Z. Kunszt, and M. Soldate, Phys. Lett. **163B**, 389 (1985); Erratum, Phys. Lett. **168B**, 427 (1986); J. F. Gunion and M. Soldate, Phys. Rev. **D34**, 826 (1986); R. K. Ellis and R. J. Gonsalves, in *Proc. of the Workshop on super high energy physics*, Eugene, OR (1985), ed. D. E. Soper, p. 287.
- [24] K. Hagiwara and D. Zeppenfeld, Nucl. Phys. **B313**, 560 (1989).
- [25] V. Barger, T. Han and J. Ohnemus, and D. Zeppenfeld, Phys. Rev. Lett. **62**, 1971 (1989); Phys. Rev. **D40**, 2888 (1989).
- [26] F. A. Berends *et al.*, Phys. Lett. **B224**, 237 (1989).
- [27] H. Chehime and D. Zeppenfeld, Phys. Rev. **D47**, 3898 (1993).
- [28] W. W. Armstrong *et al.*, Atlas Technical Proposal, report CERN/LHCC/94-43 (1994).
- [29] D. Cavalli, L. Cozzi, L. Perini, S. Resconi, ATLAS Internal Note PHYS-NO-051, Dec. 1994.
- [30] D. Rainwater, T. Plehn, and D. Zeppenfeld, preprint MADPH-99-1142 [hep-ph/9911385].